Quaternary Science Reviews 29 (2010) 1983–1992

Contents lists available at ScienceDirect

Quaternary Science Reviews

journal homepage: www.elsevier.com/locate/quascirev

Changes in atmospheric CO_2 and its carbon isotopic ratio during the penultimate deglaciation

A. Lourantou [a,1], J. Chappellaz [a,*], J.-M. Barnola [a,2], V. Masson-Delmotte [b], D. Raynaud [a]

[a] Laboratoire de Glaciologie et Géophysique de l'Environnement (LGGE, CNRS, Université Joseph Fourier – Grenoble), 54 rue Molière, Domaine Universitaire BP 96, F-38402 St Martin d'Hères Cedex, France

[b] Laboratoire des Sciences du Climat et de l'Environnement (IPSL/CEA, CNRS, Université Versailles – St Quentin), L'Orme des Merisiers, F-91191 Gif-sur-Yvette, France

ARTICLE INFO

Article history:
Received 27 November 2009
Received in revised form
8 April 2010
Accepted 1 May 2010

ABSTRACT

The largest natural increases in atmospheric CO_2 concentration as recorded in ice cores occur when the Earth climate abruptly shifts from a glacial to an interglacial state. Open questions remain regarding the processes at play, the sequences of events and their similarities along different glacial–interglacial transitions. Here we provide new combined data of atmospheric CO_2 and its carbon isotopic ratio ($\delta^{13}CO_2$) for the penultimate glacial–interglacial transition (Termination II) from the Antarctic EPICA Dome C ice core. Together with the strongest Antarctic warming, this transition bears the largest CO_2 increase (104 ppmv) of the last nine Terminations, ending with an overshoot of 21 ppmv occurring within ~300 y and leading to higher levels than those of the late pre-industrial Holocene. The full CO_2 rise is accompanied by an overall decrease of the $\delta^{13}CO_2$ minimum values, on which three positive excursions are superimposed. Peak-to-peak $\delta^{13}CO_2$ changes in our record can reach ~1‰. The ice core atmospheric $\delta^{13}CO_2$ appears more depleted by ~0.2‰ during Termination II compared to Termination I, paralleling a similar carbon isotopic depletion recorded in marine data. During both terminations, most of CO_2 and $\delta^{13}CO_2$ variations are attributed to southern ocean stratification breakdown and decreased efficiency of the biological pump. Compared to Termination I, Termination II ice core data point to different timings of decrease in iron supply and sea-ice extent, suggesting that they could account for distinct patterns of the carbon cycle.

1. Introduction

The EPICA Dome C (EDC) East Antarctic ice core provides 800 ky of climate and atmospheric composition history, corresponding to the last eight climatic cycles (Jouzel et al., 2007; Lambert et al., 2008; Loulergue et al., 2008; Lüthi et al., 2008). The overall Antarctic temperature record deduced from water isotopic measurements in ice (Masson-Delmotte et al., 2010) reveals nine saw-tooth curves with "rapid" temperature rises followed by slower temperature decreases leading to the next glacial maximum. Such pattern coincides with the $\delta^{18}O$ signal of benthic foraminifera, depicting ice volume changes and defining the Terminations, T (Sarnthein and Tiedemann, 1990). Each Termination exhibits the most dramatic natural changes of atmospheric CO_2 mixing ratio over this time scale, both in terms of magnitude and rate of change, ranging from 45 to 100 ppmv (parts per million by volume).

Several processes are involved in these large carbon-cycle variations, whose relative contributions and timing over a glacial (G)–interglacial (IG) transition are still a matter of debate. The main processes involve physical and biological mechanisms in the oceans, with a major contribution from the Southern (S) Ocean. Productivity changes could be related to fluctuations of iron supply (Archer et al., 2000; Röthlisberger et al., 2004), of the silica inventory (Ridgwell et al., 2002) or of the ratio of inorganic to organic carbon burial (rain rate ratio) in ocean sediments (Archer et al., 2000; Ridgwell, 2003). Sea surface temperature, sea-ice cover (Stephens and Keeling, 2000), the strength of the oceanic overturning circulation (Schmittner et al., 2007) in connection with upwelling changes of the S. Ocean (Anderson et al., 2009), the long-term effect of carbonate compensation (Archer et al., 2000) and the changes in terrestrial carbon storage (Joos et al., 2004) are other important candidates modulating atmospheric CO_2 on this time scale. Until now, box models (e.g. BICYCLE, Köhler et al., 2005;

* Corresponding author. Tel.: +33 (0) 4 76 82 42 64; fax: +33 (0) 4 76 82 42 01.
E-mail addresses: anna.lourantou@locean-ipsl.upmc.fr (A. Lourantou), chappellaz@lgge.obs.ujf-grenoble.fr (J. Chappellaz), valerie.masson@lsce.ipsl.fr (V. Masson-Delmotte), raynaud@lgge.obs.ujf-grenoble.fr (D. Raynaud).
[1] Now at Laboratoire d'Océanographie et du Climat: Expérimentation et Approches Numériques (LOCEAN), IPSL-UPMC, Jussieu Paris, France.
[2] Deceased.

0277-3791/$ – see front matter © 2010 Elsevier Ltd. All rights reserved.
doi:10.1016/j.quascirev.2010.05.002

Lourantou et al., 2010) or models of intermediate complexity (e.g. CLIMBER-2, Brovkin et al., 2007) have achieved in reconstructing the G–IG CO_2 rise, only by combining all above processes.

At G–IG timescales, the main carbon reservoirs interacting with the atmosphere lie in the ocean and the continental biosphere. The concomitant evolution of the stable carbon isotopic ratio $^{13}C/^{12}C$ of atmospheric CO_2 ($\delta^{13}CO_2$) helps in disentangling contributions of major CO_2 sources. For instance, enhanced biological productivity removing CO_2 from the atmosphere would lead to increased atmospheric $\delta^{13}CO_2$ values, associated with a preferential capture of the light carbon isotope during photosynthesis in the terrestrial and/or marine biosphere. An intensified vertical mixing in the S. Ocean [for instance associated with reduced buoyancy-driven Atlantic Meridional Overturning Circulation, AMOC, in the North (N.) Atlantic] would deplete atmospheric $\delta^{13}CO_2$ and cause CO_2 to increase, as it would bring at the surface CO_2-enriched waters poor in $\delta^{13}C$ (e.g. Köhler et al., 2006; Schmittner et al., 2007). An increase in sea surface temperature enriches the atmosphere in $\delta^{13}C$ and in CO_2 due to solubility effects (e.g. Heinze et al., 1991; Köhler et al., 2005). Still, the net effect on atmospheric $\delta^{13}CO_2$ through time of any carbon-cycle mechanism is usually rendered more complex due to the buffering effect of the ocean reservoir on the isotopic ratio in the atmosphere. Carbon-cycle models are thus best adapted for quantitative interpretation of the $\delta^{13}CO_2$ signal (Köhler et al., 2010).

Analyzing the same EDC ice core, Lourantou et al. (2010) produced the first detailed record of changes in the atmospheric $\delta^{13}CO_2$ covering the last deglaciation (T-I) with unprecedented accuracy and time resolution. These data nicely confirm the ~80 ppmv CO_2 increase throughout T-I, occurring in two steps interrupted by a plateau (Monnin et al., 2001). Combined with carbon-cycle box-modeling and compared with marine records, these new data have led to the conclusion that the first step of atmospheric CO_2 increase mostly involved processes in the S. Ocean, such as the stratification breakdown (releasing old carbon stored in the deep ocean) and a decreased biological pump. The CO_2 plateau is attributed in a large part to terrestrial biosphere buildup (Lourantou et al., 2010). This work aims at testing if a similar sequence of events is at play for Termination II.

Initial drivers of Terminations are thought to be changes in the Earth's orbit, with a major role either of precession (Huybers and Wunsch, 2003), obliquity (Huybers and Wunsch, 2005; Drysdale et al., 2009) or their phasing (Schulz and Zeebe, 2006). The onset and the shape of deglaciations show similarities with the millennial-scale Antarctic Isotope Maximum events (AIM, EPICA Community Members, 2006), occurring during glacial conditions, but which do not lead to glacial terminations due to the interruption caused by Dansgaard–Oeschger events in the N. Hemisphere (Wolff et al., 2009). Such scenario is corroborated by the occurrence of a rapid jump of atmospheric CH_4 usually marking the end of the Termination and thought to be associated with the resumption of the AMOC (Petit et al., 1999; Loulergue et al., 2008). One may thus expect differences between Terminations, depending on the timing of the AMOC resumption, itself possibly modulated by the ice sheet extent in the N. Hemisphere during the preceding glacial maximum (Wolff et al., 2009). As AMOC strength and the atmospheric CO_2 mixing ratio are connected through the S. Ocean ventilation, the differences between Terminations should also show up in the CO_2 signal and its isotopic signature.

T-II is known to be one of the most rapid and abrupt terminations of the late Quaternary. It is associated with the largest G–IG Antarctic temperature increase over the last 800 ky (Jouzel et al., 2007). The optimum of the subsequent interglacial (MIS 5e), is warmer than the Early Holocene by 2–5 °C in the S. Hemisphere (Bianchi and Gersonde, 2002; Jouzel et al., 2007; Masson-Delmotte et al., 2010) and by 4–5 °C in Greenland ice (North Greenland Ice Core Project Members, 2004) and in the Arctic region during summer (CAPE Last Interglacial Project Members, 2006). Higher CO_2 mixing ratios (+7 ppmv Petit et al., 1999, +13 ppmv Fischer et al., 1999) are recorded in the Vostok ice core during the MIS 5e optimum, compared to the pre-industrial Holocene (taken at 280 ppmv).

In the following, we focus on the comparison between T-I and T-II. T-II occurs under higher eccentricity and precession than T-I (Imbrie et al., 1984), leading to a more intense N. Hemisphere summer insolation maximum, preceded by a stronger S. Hemisphere summer insolation maximum (Broecker and Henderson, 1998; Schulz and Zeebe, 2006). This may explain some of T-II specificities of climatic patterns, for instance the sea level increase preceding the 65°N June maximum insolation at 127 ky BP (e.g. Waelbroeck et al., 2008). Termination I is unusual due to the occurrence of the Antarctic Cold Reversal-Bølling/Allerød/Younger Dryas sequence (Petit et al., 1999; Monnin et al., 2001; Jouzel et al., 2007), which is preceded by a major Ice Rafted Debris (IRD) event, H1. An IRD deposit is also observed during T-II, H11 (Robinson et al., 1995), but of lower intensity than H1. Dating uncertainties are significant for H11, varying from 128 to 131 ky (Lototskaya and Ganssen, 1999; Müller and Kukla, 2004; Pahnke and Zahn, 2005; Skinner and Shackleton, 2006). We also note that at some sites of the N. Atlantic, H11 appears to cover much of the transition from 140 to 128 ky BP (McManus et al., 1994; Oppo et al., 2006; Skinner and Shackleton, 2006), instead of a narrow episode just before the MIS 5e early climatic optimum (Masson-Delmotte et al., in press). Although some continental records in the N. Hemisphere suggest standstill – like conditions in the course of T-II (e.g. Sánchez-Goñi et al., 1999), in the marine realm there are indications that the AMOC was reduced during much of T-II, in contrast with T-I where it resumed at the start of the Bølling/Allerød period, possibly explaining the T-I oscillation occurrence (Carlson, 2008). Ice core records provide indicators of regional/global significance, which are directly relevant to the possible occurrence during Terminations of millennial events such as the Antarctic Cold Reversal-Bølling/Allerød/Younger Dryas sequence. The facts that throughout T-II the CH_4 signal does not oscillate and that CO_2 and δD do not show a plateau, are clear indications that T-II differs from T-I and misses such sequence at global scale. More depleted $^{13}C/^{12}C$ ratios during T-II than T-I are observed in carbon of planktic and benthic foraminifera from different ocean basins (e.g. Ninnemann and Charles, 1997; Spero and Lea, 2002; Banakar, 2005; Pena et al., 2008), with a difference amounting to ~0.4‰. An interpretation lies upon the generally reduced strength of the AMOC during T-II compared to T-I, increasing the prevalence of old deep waters and thus depleting the average carbon isotopic composition of the global ocean (Duplessy and Shackleton, 1985). An alternative explanation involves a large change in the global wind pattern affecting the supply of terrestrial light carbon to the ocean (Banakar, 2005).

Few CO_2 mixing ratio data are available over T-II, while no ice core $\delta^{13}CO_2$ record exists yet for this period. With this study, we provide the first T-II CO_2 results from the EDC core, combined with the first T-II $\delta^{13}CO_2$ data. Thanks to similar data obtained on T-I (Lourantou et al., 2010), we can qualify the similarities and differences between the two deglaciations. Such intercomparison benefits from several facts: (i) both datasets have been obtained with the same analytical system and protocol (Lourantou, 2009), (ii) they have a consistent age scale EDC3 (Loulergue et al., 2007; Parrenin et al., 2007) and (iii) they rely on the same ice core with comparable gas trapping conditions between the two Terminations. One fundamental difference relates to the physical state of gas molecules in the EDC ice covering both Terminations: while T-I

samples are located in EDC ice at depths of 345–580 m, where gas is entrapped in the form of air bubbles, T-II lies at depths of 1670–1870 m where gas is only present as air hydrates (clathrates) due to the hydrostatic pressure increase with depth. This may have potential implications on gas extraction as discussed below (Section 3.2).

After presenting the methods used in our reconstruction and the main signal features, we will evaluate to what extent the new T-II and old T-I CO_2 and $\delta^{13}CO_2$ signals bear similarities and differences with other signals notably obtained on the EDC ice core. In absence of sufficient proxy data over T-II allowing one to run carbon-cycle box-model simulations similar to those performed by Lourantou et al. (2010) for T-I, we will use a Keeling plot approach and the comparison with other proxies in ice and marine cores to propose a scenario of carbon-cycle mechanisms able to explain both CO_2 and $\delta^{13}CO_2$ patterns in the course of T-II and the start of MIS 5e.

2. Materials and methods

We used the same analytical method and protocol as in Lourantou et al. (2010). A detailed description is provided in Lourantou (2009). In short, 40–50 g of ice are placed under vacuum and crushed in a stainless steel ball mill. The extracted gas is then expanded in a 10 cm^3 sample loop. From there, an ultra pure helium stream flushes the gas through a glass trap where CO_2 is frozen out at −196 °C. The trapped CO_2 is then transferred into a low flow rate helium stream, to be cryofocused on a small volume glass capillary tubing also at −196 °C. The subsequent warming of the capillary allows the gas transfer through a gas chromatograph to separate the CO_2 from residual impurities such as N_2O and its introduction in the isotope ratio mass spectrometer IRMS (Finnigan MAT 252). The CO_2 mixing ratio in the ice samples is deduced from a linear regression between standard gas injections ($CO_2 = 260.26 \pm 0.2$ ppmv in dry air, $\delta^{13}CO_2 = -6.40 \pm 0.03$‰ versus VPDB) at different pressures and the corresponding CO_2 peak amplitude measured by the IRMS. Each sample or external standard introduction in the IRMS is bracketed with injections of a pure CO_2 standard reference gas (internal standard, ATMO MESSER, $\delta^{13}C$ of -6.5 ± 0.1‰ versus VPDB). Each ice core gas sample result consists of the mean of three consecutive measurements of the same sample gas stored in the extraction container and expanded three times. For this analytical series on T-II EDC samples, the pooled standard deviation associated with the average value of three replicate measurements of the same extracted gas amounts to 1.9 ppmv for CO_2 and 0.1‰ for $\delta^{13}CO_2$. Pooled standard deviations of $\delta^{13}CO_2$ are therefore similar for samples from T-I and T-II. However, they appear slightly larger for T-II CO_2 data compared to T-I (Lourantou et al., 2010; Table 1). These analytical observations will be discussed further in the Section 3.2 dealing with possible artifacts associated with clathrated versus bubbly ice.

On a daily basis, a systematic correction (on average −0.3‰) is applied on the carbon isotopic ratios obtained on ice samples, based on the deviation observed between several external air standard measurements and the reference CSIRO value. Ice core results are also corrected for gravitational fractionation taking place during gas diffusion between the atmosphere and the close-off depth where gas gets entrapped into bubbles. This fractionation is proportional to the mass difference between the involved gases, the one between $^{13}CO_2$ and $^{12}CO_2$ being identical to ^{15}N versus ^{14}N of N_2. Therefore $\delta^{15}N$ of N_2 data from the EDC core could be used to correct $\delta^{13}CO_2$ for gravitational fractionation. However, EDC measurements of $\delta^{15}N$ of N_2 are not yet available at sufficient resolution for T-II. We therefore rely on an empirical relationship observed between EDC $\delta^{15}N$ of N_2 and δD (Dreyfus et al., 2010) to estimate $\delta^{15}N$ of N_2 and to correct both CO_2 and $\delta^{13}CO_2$ data. The difference between both $\delta^{15}N$ corrections amounts to less than 0.01‰ for $\delta^{13}CO_2$ (see Supplementary material). For CO_2, the gravitational correction varies from 1.2 to 2.6 ppmv, while for $\delta^{13}CO_2$ it lies between 0.4‰ (MIS6) and 0.6‰ (MIS 5e).

Table 1

Period	σ CO_2	σ $\delta^{13}CO_2$	n	Reference
T-I	1.0	0.1	63	Lourantou et al., 2010
T-II	1.9	0.1	39	This study

Pooled standard deviations of CO_2 and $\delta^{13}CO_2$, calculated out of three expansions on each sample, for both deglaciation analytical series. n corresponds to the number of samples analyzed.

3. Results

3.1. Data description

We measured a total of 37 depth levels, two of them being duplicated. The new dataset provides an average 4m-depth resolution, translating into a mean time resolution of ~520 y over T-II (excluding the three MIS6 data before T-II). The resulting CO_2 and $\delta^{13}CO_2$ data are shown in Fig. 1a, c, together with CH_4 data from the same core (Loulergue et al., 2008, Fig. 1b). Similar to Monnin et al. (2001) for T-I, we divide T-II and the start of MIS 5e into seven subperiods corresponding to observed changes in the CO_2 rate of increase/decrease.

Our new data confirm the CO_2 pattern already revealed from the Vostok and Dome Fuji ice cores throughout T-II (cf. Supplementary material), characterized by a gradual increase over ~12 ky ending up with a rapid jump toward the optimum at the start of MIS 5e. The better precision of our EDC record furthermore reveals that the abrupt CO_2 rise takes place within only ~300 yr and is

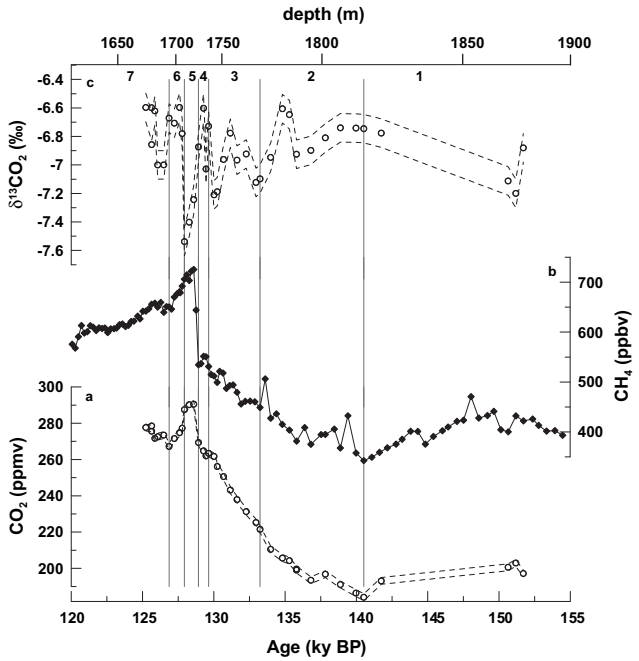

Fig. 1. Evolution of (a) CO_2, (b) CH_4 and (c) $\delta^{13}CO_2$ in the EPICA Dome C ice core throughout the penultimate deglaciation (i.e. from MIS6 to MIS 5e). CH_4 data from Loulergue et al. (2008); CO_2 and $\delta^{13}CO_2$ data from this study; mean value of error bars added as min and max dotted lines. Vertical lines mark the limit between different sub-periods, each one corresponding to a specific CO_2 rate of change. The gas time scale is EDC3_gas_a (Parrenin et al., 2007; Loulergue et al., 2007).

synchronous with the CH_4 overshoot. We show that the CO_2 overshoot is accompanied by a rapid drop of $\delta^{13}CO_2$, while throughout the entire deglaciation the isotopic signal shows a decreasing trend of its minimum values of 0.8‰ accompanying the CO_2 rise, on which three maxima are superimposed.

In the following, we detail the structure of both signals. We first compare the glacial (140 ky, n = 2) and interglacial (128 ky, n = 3) CO_2 optima defining T-II boundaries in our record. With our current time resolution, minimal (maximal) CO_2 levels amount to 185 ± 3 ppmv (289 ± 3 ppmv) whereas the corresponding $\delta^{13}CO_2$ values are −6.7 ± 0.1‰ (−7.4 ± 0.1‰), leading to a full CO_2 increase of 104 ppmv, i.e. the largest deglacial CO_2 increase of the last 9 Terminations. The full glacial–interglacial $\delta^{13}CO_2$ magnitude is only reached later, with the most depleted values found just after the CO_2 overshoot, leading to a full $\delta^{13}CO_2$ decrease of 0.8‰.

Based on the division into sub-periods related with the CO_2 rate of change, the two signals present the following trends:

1. A ~16 ppmv decrease of CO_2 and a 0.3‰ rise of $\delta^{13}CO_2$ take place at the end of MIS6 (n = 3). Given the small amount of data for the time period between 153 and 141 ka, there might exist higher variability in CO_2 and $\delta^{13}CO_2$ in-between, which cannot be resolved with the current dataset.
2. From 141 to 134 ky, CO_2 increases slowly by 26 ppmv while $\delta^{13}CO_2$ first declines by about 0.2‰ and then shows a ~0.3‰ positive peak over a duration of ~2 ky.
3. The following ~4 ky (from 134 to 130 ky) are characterized by a more rapid CO_2 rise of ~50 ppmv accompanied by another positive $\delta^{13}CO_2$ peak with an amplitude of ~0.3‰, superimposed on a slightly lower $\delta^{13}CO_2$ background compared with the previous sub-period.
4. Between 130 and 129 ky, the CO_2 mixing ratio barely increases by 8 ppmv (60% of this increase occurring within the last 350 y), while $\delta^{13}CO_2$ reveals two sharp peaks with an amplitude reaching 0.6‰.
5. The following ~1 ky is first marked by an unusually abrupt and large CO_2 increase (overshoot of 21 ppmv in ~300 y). The corresponding rate of increase, of 0.06 ppmv/y, is two to three times larger than the most rapid increases observed during T-I, at the beginning of the Bølling–Allerød, and at the end of the Younger Dryas (Monnin et al., 2001), and ten times larger than the rate of increase accompanying the ~20-ppmv rise observed during rapid events of the last glaciation, such as the AIM events (Ahn and Brook, 2008). It is however much lower than during the Anthropocene (~2ppmv/y). Such rate of increase may be slightly underestimated due to the time resolution of our measurements and due to the smoothing of atmospheric variations by the enclosure process of air into ice at Dome C (interglacial width of age distribution of ~200 y, Joos and Spahni, 2008), being close to the time resolution of the depicted overshoot. The overshoot is followed by a CO_2 plateau at 289 ± 3 ppmv during ~700 y, at a level significantly larger than observed during the pre-industrial Holocene. Such feature is also observed during MIS 9 (Petit et al., 1999). The overshoot and the subsequent plateau are accompanied by a strong negative $\delta^{13}CO_2$ excursion of ~0.7‰, reaching the most negative values observed throughout the Termination, i.e. −7.5‰.
6. From 128 to 127 ky, CO_2 reveals a 20-ppmv decline, taking place in two steps: an initial rapid decline of 10 ppmv within 160 y, followed by a slower one of 10 ppmv within ~900 y. The rapid decline is accompanied by a very large $\delta^{13}CO_2$ increase of ~0.8‰, reaching again the largest level observed throughout the Termination.
7. The last ~1.6 ky of our record progressing into MIS 5e show a slow 10-ppmv rise accompanied with a negative $\delta^{13}CO_2$ oscillation of ~0.3‰.

CH_4 shows similar patterns as CO_2 for T-II, with no apparent anti-correlation, contrary to what was observed during the last two sub-periods of T-I (Monnin et al., 2001; Lourantou et al., 2010). An important difference is encountered after 126 ky, where they follow opposing trends (increase for CO_2 and decrease for CH_4, Fig. 1a,b). The atmospheric $\delta^{13}CO_2$ signal experienced salient peaks and troughs within all defined sub-periods (Fig. 1c), features which are not always associated with a major change in CO_2 mixing ratio or its rate of increase/decrease, contrary to observations of Lourantou et al. (2010) over T-I. The amplitude of $\delta^{13}CO_2$ changes over T-II also appears larger than during T-I. The $\delta^{13}CO_2$ signal reveals no apparent correlation with CH_4 throughout T-II (Fig. 1b,c), contrary to what is found in the end of T-I (Lourantou et al., 2010).

3.2. Bubbly against clathrated ice

In the depth range of the T-II EDC ice samples, the trapped gases only exist in the form of clathrates. Clathrates are strongly linked with the molecular network of the ice matrix. The dissociation of CO_2 clathrates into free gas plus H_2O is impeded compared with e.g. CH_4 clathrates (Circone et al., 2003). One could hypothesize that dry extraction methods applied on ice cores (i.e. mechanical ice grinding at negative temperature) could eventually fractionate the CO_2 mixing ratio between released and unreleased gases from clathrates, depending for instance on the final grain size of the grinded ice powder. Due to the different equilibrium pressure of pure hydrates made of different CO_2 isotopologues, such fractionation might also affect $\delta^{13}CO_2$ in the released gases. Lower δD has been reported on guest CH_4 and C_2H_6 molecules in clathrates compared with the residual free gas (Hachikubo et al., 2007), thus confirming the possibility of isotopic fractionation between clathrates and free gas. In general, the crushing process easily releases atmospheric gases trapped in structural voids in the ice (such as bubbles or cracks) but can be less effective in releasing gases which are encaged in the molecular structure of the ice (Anklin et al., 1997; Wilson and Long, 1997; Stauffer and Tschumi, 2000).

This phenomenon indeed clearly shows up when comparing the extraction efficiency of our method on T-I and T-II EDC samples (data of T-I taken from Lourantou et al., 2010). In Fig. 2, we compare the amount of gas released from the EDC samples with our extraction technique (expressed in cm^3 STP of dry air per g of ice, see appendix for the calculation) with the air content of neighboring EDC samples measured with an absolute method involving melting and refreezing of the ice (Lipenkov et al., 1995; Raynaud et al., 2007). The amount of gas released with the dry extraction method is lower by more than 20% on T-II EDC samples compared with the T-I ones (on average 0.047 ± 0.006 cm^3/g against 0.060 ± 0.005 cm^3/g for T-II and T-I, respectively), whereas the true air content of the ice slightly increases by ~3% (mean of 0.092 ± 0.003 cm^3/g vs. 0.089 ± 0.003 cm^3/g for T-II and T-I, respectively, Fig. 2). We deduce a grinding efficiency (ratio between released gas and air content) of 62% for the ice samples covering the T-I period, and of only 52% for the T-II samples. The dry extraction method is thus less efficient on 100% clathrated ice than on 100% bubbly ice, as previously proposed (Wilson and Long, 1997) and as observed on NGRIP samples using the Bern needle cracker (Stauffer and Tschumi, 2000).

We then need to evaluate if this reduced efficiency affects the composition of the released air compared with the trapped gases. Table 1 compares the scattering calculated on the three consecutive

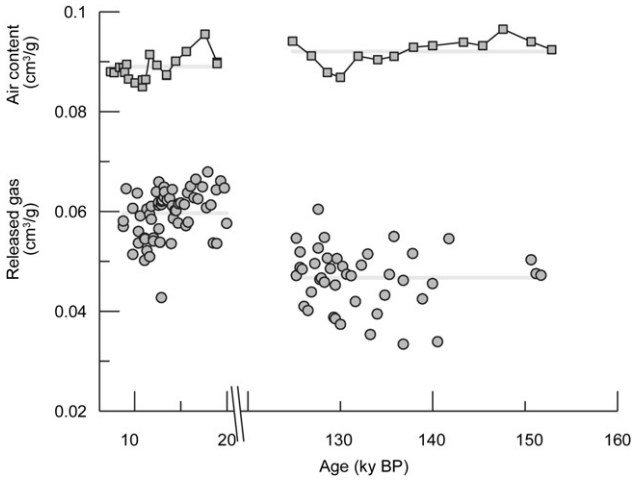

Fig. 2. Comparison between T-I (left) and T-II (right) air content of EDC ice as measured with an absolute method (Raynaud et al., 2007, upper plot) and the amount of released gas measured after dry crushing of our samples (lower plot). In the four panels, the bold grey line indicates the average over the period of concern.

expansions of the extracted gas on ice samples for both CO_2 and $\delta^{13}CO_2$ measured over T-I and T-II. The CO_2 dispersion is higher by ~50% on T-II samples compared with T-I, with a tendency for CO_2 to slightly increase with subsequent expansions, whereas the $\delta^{13}CO_2$ scattering between the two sets of samples is comparable. Recent experiments were conducted with the LGGE dry extraction system, comparing 100% bubbly ice from the Berkner Antarctic ice core with EDC ice of the same gas age but in which trapped gases co-exist as clathrates and free gas in bubbles (transition zone known as "brittle ice"). These tests have shown a significant depletion of CO_2 in the gas released from the EDC ice, by ~12 ppmv (Schaefer et al., in preparation). They also revealed a large CO_2 dispersion (by more than 100%) compared to T-I data. On the other hand, no significant differences were detected for $\delta^{13}CO_2$ results. Such artifact observed on brittle ice, affecting the CO_2 mixing ratio but not its $\delta^{13}C$, cannot be directly translated to the case of 100% clathrated ice; it could nevertheless provide an upper limit of the possible bias due to the gas extraction technique. Recently, CO_2 analyses of 100% clathrated EDC ice were also performed in deeper layers of the core using two techniques: our dry extraction one and the Bern sublimation technique (providing 100% extraction efficiency, and thus not affected by bubble-hydrate transformation). They agree very well on adjacent depth levels, within a 2–5 ppmv range (Lüthi et al., 2008). This suggests that, if any, the bias introduced by our method on CO_2 mixing ratio on 100% clathrated ice amounts to less than 5 ppmv, while there is no evidence to date of possible effect on $\delta^{13}CO_2$.

We conclude that even if the extraction efficiency of our method is lower on 100% clathrated ice compared to 100% bubbly ice, this may induce a slight underestimation in the measurement of CO_2 mixing ratio in ice, but should not affect the $\delta^{13}CO_2$ signal. In the following, the main structure of both signals throughout T-II is thus assumed to be valid and is further discussed in terms of carbon-cycle mechanisms and climate dynamics.

4. Discussion

4.1. Comparison of CO_2, CH_4 and $\delta^{13}CO_2$ patterns during Terminations I and II

The three gas signals can be directly compared in terms of phasing and shape, as they are obtained on the same matrix. CH_4 is closely related to Greenland and more generally N. Hemisphere climate (e.g. Chappellaz et al., 1993; Brook et al., 1996); in addition, model simulations show that Greenland climate was largely modulated by AMOC changes (e.g. Otto-Bliesner and Brandy, 2010 and references therein). The comparison of CH_4 with CO_2 and $\delta^{13}CO_2$ thus possibly brings hints into the carbon-cycle processes related to AMOC dynamics, An intensified hydrological cycle producing more CH_4 on the continents (Fischer et al., 2008) should also be associated with a stronger carbon uptake through continental biomass buildup, notably in peatlands (Frolking and Roulet, 2007). Throughout T-II, CH_4 depicts two distinct features: a slow and regular increase from 141 to 129 ky, and a rapid increase during the ~300 y preceding the optimum of MIS 5e. Such evolution goes in line with the scenario where the AMOC was dampened during much of T-II and strengthened very rapidly at 129 ky (Carlson, 2008). Parallel to the CH_4 evolution, CO_2 increases in a similar manner which can be schematized as a long and relatively steady increase (albeit with some fluctuations highlighted by the subperiods) culminating with the overshoot at 129 ky. It thus bears resemblance with the first half of T-I (from 17.6 to 14.7 ky) with a slow increase of both signals leading to the Bølling/Allerød warming and the first CH_4 and CO_2 rapid jumps, but on a ~fourfold longer duration and a much larger amplitude: 55 ppmv for the first half of T-I versus 104 ppmv for the entire T-II.

The full T-II amplitude of change for CO_2 and CH_4 is also much larger than T-I (Fig. 3a,b): 104 ppmv (385 ppbv) compared with 82 ppmv (335 ppbv) (Loulergue et al., 2008; Lourantou et al., 2010). The overall CO_2 rise throughout T-II is accompanied by a large decline of the $\delta^{13}CO_2$ minimum values, culminating at the time of the CO_2 overshoot. It bears resemblance with the first half of T-I as well, albeit with much larger amplitude: 0.8‰, instead of 0.6‰ during the first half (and throughout, as well) of T-I (Fig. 3g).

Although $\delta^{13}CO_2$ exhibits a large variability during both Terminations, we observe a statistically significant difference of its average value, the mean $\delta^{13}CO_2$ during the time period 125–140 ky BP being 0.2‰ more depleted than during the time period 9–22 ky BP. Such feature of more ^{13}C-depleted carbon in the atmosphere during the penultimate deglaciation than the most recent one goes in parallel with a similar ^{13}C depletion in the oceanic reservoir, seen in planktic and benthic foraminifera from different ocean basins (Duplessy and Shackleton, 1985; Seidenkrantz et al., 1996; Ninnemann and Charles, 1997; Hendy and Kennett, 2000; Molyneux et al., 2007; Pena et al., 2008), albeit with a larger amplitude of ~0.4‰. The oceanic ^{13}C depletion was interpreted as resulting from an even more reduced AMOC strength during T-II, increasing the prevalence of old deep waters and depleting the average carbon isotopic composition of the global intermediate ocean (Duplessy and Shackleton, 1985). The fact that it parallels a ^{13}C depletion in the atmospheric reservoir suggest that T-II and the preceding glacial maximum experienced an even more reduced carbon storage on the continents, compared with T-I and the LGM, thus transferring more ^{13}C-depleted carbon in the two other reservoirs.

The CH_4, CO_2 and $\delta^{13}CO_2$ comparison between the two Terminations reinforce the scenario of reduced AMOC during T-II until the abrupt increase of both greenhouse gases at the very end of the Termination, when AMOC would have intensified. This is in line with the sequence of events discussed by Monnin et al. (2001) for interpreting the T-I CO_2 evolution, and in accordance with modeling studies on the impact of AMOC perturbations on atmospheric CO_2, under initial pre-industrial conditions (Menviel et al., 2008).

4.2. Comparison with other ice and marine core records

In our previous work on T-I, we had compared atmospheric composition records with marine data which document in detail

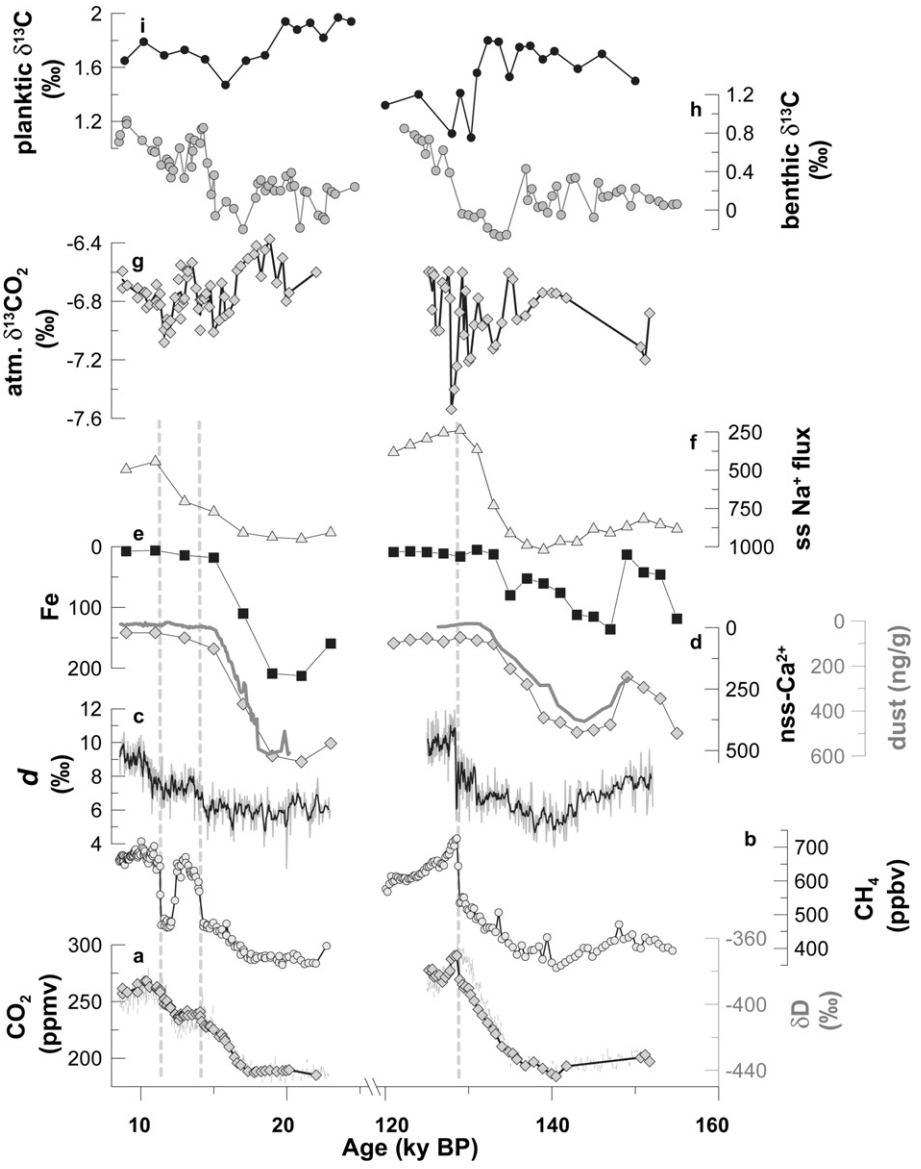

Fig. 3. Comparison of T-I and T-II for a range of proxies: (a) atmospheric CO_2 measured on EDC ice (Lourantou et al., 2010 and this study), superimposed on EDC δD (grey dotted line, Jouzel et al., 2007); (b) atmospheric CH_4 (Loulergue et al., 2008); (c) deuterium excess *d* (Masson-Delmotte et al., in press) with a running average (darker line); (d) non sea-salt Ca^{2+} from EDC ice (diamonds) superposed with EDC dust (line, running average over 1600 y for T-I, 3000 y for T-II; Lambert et al., 2008); (e) Fe flux from EDC ice (Gaspari et al., 2006); (f) sea-salt Na^{+} from EDC ice (Wolff et al., 2006); (g) atmospheric $\delta^{13}CO_2$ (Lourantou et al., 2010 and this study); (h) benthic $\delta^{13}C$ on the Iberian margin (Skinner and Shackleton, 2006); (i) planktic $\delta^{13}C$ from the eastern equatorial Pacific (Spero and Lea, 2002). Ice core data are on the EDC3 age scale (Parrenin et al., 2007), while marine data are plotted on their own timescales.

the evolution of some of the key players coupling atmospheric CO_2 and global climate. Dating uncertainties and fewer available records render a similar implementation difficult on T-II. In Fig. 3, we take advantage of the different proxies from marine and ice core realm and compare them between both deglaciations. The temporal evolution of these signals can be compared, keeping in mind absolute dating uncertainties which reach 3 ky for the EDC ice core over T-II (Parrenin et al., 2007) and ~1 ky between the gas and ice signals (Loulergue et al., 2007).

Fig. 3a shows a co-variation of CO_2 with δD (reflecting high southern latitude temperature) throughout T-II. This suggests that CO_2 changes are controlled by the S. Ocean during the penultimate deglaciation, as was deduced from the co-variation over T-I (Monnin et al., 2001). The EPICA Dome C ice core also provides records of dust (nss-Ca^{2+}, Fig. 3d) and sea-ice extent (ss-Na^{+}, Fig. 3f). These proxy records show systematic sequences of events with Antarctic temperature (δD) during all glacial terminations (Röthlisberger et al., 2008). All the ice core records exhibit differences in magnitude and structure between T-I and T-II (Fig. 3a–g). Regarding amplitudes of change characterizing T-II, we observed the following compared to T-I: in addition to the +22 ppmv for CO_2 (Fig. 3a), +50 ppbv for CH_4 (Fig. 3b) and −0.2‰ for $\delta^{13}CO_2$ (Fig. 3g) mentioned before, δD increases by an additional 18‰ (Fig. 3a), *d*-excess by +1.2‰ (Fig. 3c), and ss-Na^{+} rises by an extra 270 μg/m^2/y (Fig. 3f). Only does the range of dust flux, whatever the proxy used (dust, iron, nss-Ca^{2+}, Fig. 3d,e) appear weaker for T-II than T-I, probably due to warmer S. Hemisphere temperatures, related to the reduced AMOC.

As seen for CO_2, δD does not depict an Antarctic Cold Reversal-like feature during T-II, but it differs from the CO_2 evolution during

the late part of T-II, with a monotonic increase whereas CO_2 shows first a slowing-down of its rate of increase and then an abrupt jump at 129 ky BP. On the other hand both signals peak at approximately the same time (Fig. 3a). The rapid CO_2 jump parallels a similar feature in the *d*-excess record, a proxy of moisture source which suggests a shift toward lower latitudes associated with weakened westerlies (Masson-Delmotte et al., in press). The parallelism between both signals suggests that the CO_2 overshoot could find in part its origin in abruptly reduced westerlies associated with a shift in moisture source as well. The direction of westerlies shifts on a G–IG transition is, however, highly controversial: Zharkov and Nof (2008) support a northward G–IG shift, in contrast to Toggweiler et al. (2006) who assume a poleward movement. The latter assumption enhances upwelling and therefore could be responsible for propagating the deep ocean signal to the atmosphere, under the condition that there is no sea-ice impeding this process. Fig. 3f shows the lowest fluxes of the sea-ice proxy (Na^+) at exactly that time frame, while in Fig. 3i, planktic $\delta^{13}C$ data show a minimum at the same time, possibly reflecting enhanced upwelling (Spero and Lea, 2002). Since the upwelling may drive a large atmospheric CO_2 rise and $\delta^{13}CO_2$ decline, our data are thus in line with the Toggweiler et al. (2006) scenario to explain at least partly the ~20 ppmv CO_2 overshoot at the start of MIS 5e.

Although the amplitude of dust change appears less important during T-II than T-I whatever the proxy used (dust, iron, nss-Ca^{2+}), elevated dust levels persist longer during T-II than T-I. The dust supply in the S. Ocean has been active during 10 ky for T-II, corresponding to a CO_2 increase of 50 ppmv, to compare with the 4-ky duration of the elevated dust concentration during T-I associated with a 35-ppmv CO_2 rise (Fig. 3d). The Fe fertilization effect (Martin, 1990) could thus account for a significant part of the initial CO_2 increase, associated with negative atmospheric $\delta^{13}CO_2$ trend, observed during T-II as well as the early part of T-I (Lourantou et al., 2010). The benthic $\delta^{13}C$ profile from the Iberian margin, shown in Fig. 3h, reflects changes in deep-water ventilation in the N.E. Atlantic (Skinner and Shackleton, 2006). The W-pattern seen for T-I, as in the atmospheric $\delta^{13}CO_2$ signal, is absent during T-II. An abrupt decline, followed by a more gradual increase is observed for T-II, whereas the atmospheric $\delta^{13}CO_2$ signal shows more abrupt shifts.

The whole atmospheric $\delta^{13}CO_2$ decreasing trend is punctuated by three peaks, the older two not being clearly associated with an important CO_2 feature apart from the small change in its rate of increase. These peaks might have been related to abrupt sea surface temperature changes (Fig. 3a,g), as discussed below.

4.3. Scenarios of carbon-cycle evolution

The comparison above between CO_2, $\delta^{13}CO_2$ and other proxies relevant to the carbon-cycle evolution during T-II suggests that similar mechanisms as during the first half of T-I took place to generate first a gradual increase of CO_2 and decrease of $\delta^{13}CO_2$, and then a CO_2 overshoot ending the $\delta^{13}CO_2$ decrease: a reduced AMOC (even more reduced than during T-I) favored stronger ventilation of the S. Ocean, releasing $\delta^{13}C$-depleted CO_2, a mechanism accompanied by sea-ice retreat but also by a decrease in iron aeolian input extending through a longer part of T-II than observed during T-I (reducing the biological pump strength). At the end of the Termination, the AMOC strengthening would have taken place in parallel to a poleward shift of the westerlies, resulting into the rapid CO_2 jump. In order to evaluate such scenarios, a useful – albeit limited – approach consists in using a Keeling plot and comparing with its equivalent for T-I (Lourantou et al., 2010). In a two-reservoir system, Keeling plots allow one to deduce the carbon isotopic composition of the source adding CO_2 in the second reservoir, i.e. the atmosphere, when plotting $\delta^{13}CO_2$ as a function of the inverse of CO_2. It is not very appropriate for a three-reservoir system (biosphere–ocean–atmosphere), due to the buffering effect of the ocean modifying the *y*-intercept of the regression between both variables (Köhler et al., 2006). But, qualitatively, a Keeling plot can highlight processes at play and similarities between the two deglaciations.

Fig. 4a compares Keeling plots of both Terminations. We calculate the *y*-intercept for each rapid period of $\delta^{13}C$ decline associated with a CO_2 increase (two for T-I and three for T-II). It lies between −11 and

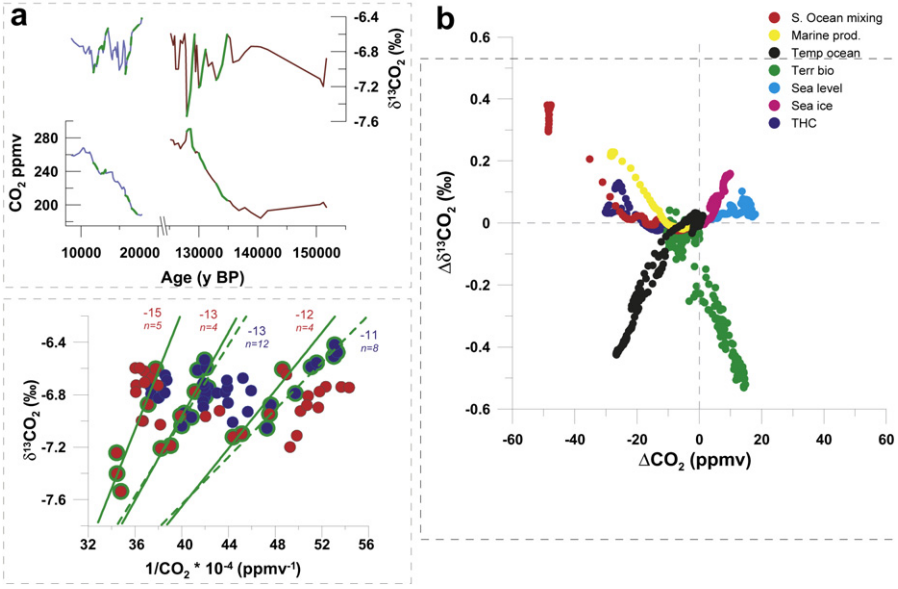

Fig. 4. a. Left panel: upper graph: color coding of different sequences of $\delta^{13}CO_2$ and CO_2 evolution during T-I and T-II; abrupt $\delta^{13}CO_2$ declines are highlighted in green. Lower graph: Keeling plot for both T-I (blue circles) and T-II (red circles). The continuous (T-II) and dashed (T-I) lines indicate linear regression through the selected data (green lines in the upper graph). The value of the *y*-intercept is given next to each regression line, together with the number of data points used. b. Right panel: Co-evolution of $\delta^{13}CO_2$ and CO_2 sources/sinks depending on different carbon-cycle mechanisms simulated in the course of T-I with the carbon box-model BICYCLE (Köhler et al., 2005, figure adapted from simulations presented in Lourantou et al., 2010). (For interpretation of the references to color in this figure legend, the reader is referred to the web version of this article.)

−15‰, i.e. a relatively narrow range for both deglaciations, suggesting a common mechanism behind the corresponding CO_2 phases of increase. Lourantou et al. (2010), using the BICYCLE box-model, associated these "Keeling-plot" signatures with a physical mechanism (the breakdown of S. Ocean stratification), combined with a biological process (a decreased biological pump) for the first step of $\delta^{13}CO_2$ reduction. The Keeling plot approach suggests that such mechanisms could also explain a large part of the T-II CO_2 increase. Only the physical processes can be invoked during the rapid jump of CO_2 at 129 ky BP, as the dust/iron levels in EDC already reached interglacial low levels before this particular CO_2 event.

Still, a stringent observation in the CO_2–$\delta^{13}CO_2$ co-evolutions during T-II is the occurrence of three $\delta^{13}CO_2$ peaks superimposed on its large decline, accompanied by only small changes in the rate of CO_2 increase for two of them. Such feature seems present also during sub-period II of the last deglaciation, when H1 occurred, with two small $\delta^{13}CO_2$ peaks when the CO_2 rate of increase also shows minor changes. These positive $\delta^{13}CO_2$ peaks produce a much more positive *y*-intercept in the Keeling plot (not shown in Fig. 4). Fig. 4b gives the combined evolution of $\delta^{13}CO_2$ and the CO_2 source/sink resulting from different carbon-cycle mechanisms, simulated in the course of T-I with the carbon box-model BICYCLE (Köhler et al., 2005, graph adapted from simulations in Lourantou et al., in press). Among them, three processes are able to associate a CO_2 increase with a positive $\delta^{13}CO_2$ anomaly: (1) increasing SSTs, (2) decreasing sea-ice cover and (3) sea level rise. The last one is probably too slow to generate $\delta^{13}CO_2$ anomalies at time-scales of 2 ky or less, as observed during T-II. It thus seems plausible that positive excursions in our $\delta^{13}CO_2$ reflects periods of rapidly changing sea surface conditions in areas of important CO_2 exchange.

In summary, although the lack of proxy data from the marine and continental realms and of carbon-cycle modeling applied to T-II seriously limits the strength of our conclusions, the combination of CO_2 and $\delta^{13}CO_2$ evolutions in the course of the penultimate deglaciation suggests that S. Ocean stratification breakdown and decreased biological pump could well explain the main features observed in the two signals. In particular the delayed decrease (compared to T-I) of dust input and sea-ice cover suggested by the EDC ice proxies points toward a relatively stronger contribution of associated carbon-cycle mechanisms. Such delay could potentially be related to the differences in orbital configuration (e.g. Broecker and Henderson, 1998) and ice sheet extent (e.g. Govin et al., submitted for publication), affecting the strength of AMOC, notably reduced during MIS 6 and T-II compared with MIS 2 and T-I, as suggested by $\delta^{13}C$ records in the world oceans. This could justify why (1) the amplitude of the CO_2 increase and $\delta^{13}CO_2$ decrease are much larger than T-I and (2) the CO_2 increase ends up with a large 21-ppmv jump in ~300 y. The latter could find an additional contribution through intensified upwelling, due to a poleward shift of the westerlies which contributes as well to the extent of tropical wetlands, leading to concomitant and rapid increases of both CO_2 and CH_4.

Positive $\delta^{13}CO_2$ excursions superimposed on the long-term decrease along T-II suggest that rapid changes in sea surface temperature and sea-ice extent could also have contributed to the 104 ppmv rise. It is only after the CO_2 optimum of MIS 5e, when CO_2 decreases by ~10 ppmv and $\delta^{13}CO_2$ increases back to its highest level (sub-period 6), that the co-evolution of both signals goes in line with a possible contribution from vegetation buildup, taking away CO_2 from the atmosphere and leaving a more enriched $\delta^{13}C$ signature, as suggested by Lourantou et al. (2010) for the Bølling/Allerød sequence during T-I.

5. Conclusions

The new dataset of CO_2 and $\delta^{13}CO_2$ from the EDC ice core over the penultimate deglaciation presented here, provides important quantitative constraints on climate/carbon-cycle interactions during this major climatic event. It confirms that the CO_2 increase (of 104 ppmv in our record) is the largest observed over the last 9 Terminations. This increase takes place in two major steps: a long increase from 141 to 129 ky BP, accompanied by minor changes in the rate of increase, and a rapid jump (21 ppmv in ~300 y) toward the MIS 5e maximum, taking place at 129 ky BP. This is accompanied by large variations of $\delta^{13}CO_2$, which can be sketched as a progressive decrease of the minimum values through time, culminating when CO_2 jumps to its maximum at 129 ky BP, and three positive excursions superimposed on the long trend. The larger amplitudes encountered in our atmospheric signals are also seen in other ice core proxy records. The more depleted (by 0.2‰) average atmospheric $\delta^{13}CO_2$ signal during T-II compared with T-I is also witnessed in marine sediments, and suggests a larger transfer of ^{13}C-depleted carbon from the terrestrial reservoir to the ocean–atmosphere ones before and during T-II.

A first attempt to interpret these records using Keeling plots, and a comparison with other ice core and marine data covering the past two deglaciations, suggest that S. Ocean upwelling combined with reduced biological pump could have been the two dominant factors controlling CO_2 levels throughout T-II as during the first half of T-I. The continental biosphere would have left an imprint in both CO_2 and $\delta^{13}CO_2$ only after the optimum of MIS 5e. The main differences between the two Terminations could be summarized as: (1) a delayed response of dust and sea-ice decreases in the course of T-II and a reduced AMOC, contributing to increase even more CO_2 in the atmospheric reservoir and (2) the lack of a millennial-scale event similar to the Antarctic Cold Reversal-Bølling/Allerød-Younger Dryas sequence, most probably due to different boundary conditions of ice sheet extents. Additional proxy information from high-resolution sediment records covering this critical period (e.g. more detailed records on the occurrence of H11 event and the final AMOC resumption), as well as the use of carbon-cycle models will help in verifying the above assumptions and better deciphering the mechanisms at play. Lastly, even if there is no indication that the dataset presented here would be affected by any known artifact, future measurements performed using different techniques and on different ice cores will be helpful to confirm the main features seen in our record.

Acknowledgments

This work is a contribution to the European Project for Ice Coring in Antarctica (EPICA), a joint ESF (European Science Foundation)/EC scientific program, funded by the European Commission and by national contributions from Belgium, Denmark, France, Germany, Italy, the Netherlands, Norway, Sweden, Switzerland and the United Kingdom. The main logistic support was provided by IPEV and PNRA (at Dome C). AL was funded by the European Research Training and Mobility Network GREENCYCLES. Additional funding support was provided by the QUEST-INSU project DESIRE, the FP6 STREP EPICA-MIS, and the French ANR PICC (ANR-05-BLAN-0312-01). This work was also supported by funding to the Past4Future project from the European Commission's 7th Framework Programme, grant number 243908, and is Past4Future contribution number 3. Long-term support for the mass spectrometry work at LGGE was provided by the Fondation de France and the Balzan Price of C. Lorius. We thank G. Dreyfus for providing nitrogen isotopic data. Discussions with Peter Köhler, Maria-Fernanda Sanchez-Goni, Eric Wolff, Laurent Labeyrie, Andrew Friend and Philippe Ciais were very much appreciated. The authors also thank two anonymous

reviewers for their fruitful comments on a previous version of this manuscript.

This is EPICA publication n°266.

Appendix. Calculation of the amount of air released from ice core samples after milling

$$V/m = \left[\frac{V_m - V_{ice}}{T_{m,1}} + \frac{V_l}{T_{l,1}}\right] \times \frac{T_0}{P_0 \times m} \times (P_1 - P_{H_2O})$$

where V represents the amount of air released, m represents the sample mass, T the temperature, P the extraction pressure, P_{H_2O} the pressure of water vapour, T_0 273 K and P_0 1013 hPa (standard conditions). The subscript l corresponds to the extraction line, m to ice mill, and the number "1" indicates the 1st sample expansion.

Appendix. Supplementary material

Supplementary data associated with this article can be found, in the on-line version, at doi: 10.1016/j.quascirev.2010.05.002.

References

Ahn, J., Brook, E.J., 2008. Atmospheric CO_2 and climate on millennial time scales during the last glacial period. Science 322, 83–85.

Anderson, R.F., Ali, S., Bradtmiller, L.I., Nielsen, S.H.H., Fleisher, M.Q., Anderson, B.E., Burckle, L.H., 2009. Wind-driven upwelling in the Southern Ocean and the deglacial rise in atmospheric CO_2. Science 323, 1443–1448.

Anklin, M., Schwander, J., Stauffer, B., Tschumi, J., Fuchs, A., Barnola, J.M., Raynaud, D., 1997. CO_2 record between 40 and 8 kyr B.P. from the Greenland Ice Core Project ice core. Journal of Geophysical Research 102, 26539–26545.

Archer, D., Winguth, A., Lea, D., Mahowald, N., 2000. What caused the glacial/interglacial atmospheric pCO_2 cycles? Reviews of Geophysics 38, 159–190.

Banakar, V.K., 2005. Delta 13C depleted oceans before the termination 2: more nutrient-rich deep-water formation or light-carbon transfer? Indian Journal of Marine Sciences 34, 249–258.

Bianchi, C., Gersonde, R., 2002. The Southern Ocean surface between Marine Isotope Stages 6 and 5d: shape and timing of climate changes. Palaeogeography, Palaeoclimatology, Palaeoecology 187, 151–177.

Broecker, W.S., Henderson, G.M., 1998. The sequence of events surrounding termination II and their implications for the cause of glacial–interglacial CO_2 changes. Paleoceanography 13, 352–364.

Brook, E., Sowers, T., Orchardo, J., 1996. Rapid variations in atmospheric methane concentration during the past 110,000 years. Science 273, 1087–1091.

Brovkin, V., Ganopolski, A., Archer, D., Rahmstorf, S., 2007. Lowering of glacial atmospheric CO_2 in response to changes in oceanic circulation and marine biogeochemistry. Paleoceanography 22, PA4202. doi:10.1029/2006PA001380.

CAPE Last Interglacial Project Members, 2006. Last Interglacial Arctic warmth confirms polar amplification of climate change. Quaternary Science Reviews 25, 1383–1400.

Carlson, A.E., 2008. Why there was not a Younger Dryas-like event during the Penultimate Deglaciation. Quaternary Science Reviews 27 (9–10), 882–887.

Chappellaz, J., Blunier, T., Raynaud, D., Barnola, J.-M., Schwander, J., Stauffer, B., 1993. Synchronous changes in atmospheric CH4 and Greenland climate between 40 and 8 kyr BP. Nature 366, 443–445.

Circone, S., Stern, L.A., Kirby, S.H., Durham, W.B., Chakoumakos, B.C., Rawn, C.J., Rondinone, A.J., Ishii, Y., 2003. CO_2 hydrate: synthesis, composition, structure, dissociation behavior, and a comparison to structure I CH_4 hydrate. Journal of Physical Chemistry B 107, 5529–5539.

Dreyfus, G.B., Jouzel, J., Bender, M.L., Landais, A., Masson-Delmotte, V., Leuenberger, M., 2010. Firn processes and δ15N: potential for a gas-phase climate proxy. Quaternary Science Reviews 29, 28–42.

Drysdale, R.N., Hellstrom, J.C., Zanchetta, G., Fallick, A.E., Sanchez-Gõni, M.F., Couchoud, I., McDonald, J., Maas, R., Lohmann, G., Isola, I., 2009. Evidence for obliquity forcing of glacial termination II. Science 325, 1527–1531.

Duplessy, J.-C., Shackleton, N.J., 1985. Response of global deep-water circulation to Earth's climatic change 135,000–107,000 years ago. Nature 316, 500–507.

EPICA Community Members, 2006. One-to-one coupling of glacial climate variability in Greenland and Antarctica. Nature 444, 195–198.

Fischer, H., Wahlen, M., Smith, J., Mastroianni, D., Deck, B., 1999. Ice core records of atmospheric CO_2 around the last three glacial terminations. Science 283, 1712–1714.

Fischer, H., Behrens, M., Bock, M., Richter, U., Schmitt, J., Loulergue, L., Chappellaz, J., Spahni, R., Blunier, T., Leuenberger, M., Stocker, T.F., 2008. Changing boreal methane sources and constant biomass burning during the last termination. Nature 452, 864–867.

Frolking, S., Roulet, N.T., 2007. Holocene radiative forcing impact of northern peatland carbon accumulation and methane emissions. Global Change Biology 13 (5), 1079–1088.

Gaspari, V., Barbante, C., Cozzi, G., Cescon, P., Boutron, C.F., Gabrielli, P., Capodaglio, G., Ferrari, C., Petit, J.R., Delmonte, B., 2006. Atmospheric iron fluxes over the last deglaciation: climatic implications. Geophysical Research Letters 33, L03704. doi:10.1029/2005GL024352.

Govin, A., Braconnot, P., Capron, E., Cortijo, E., Duplessy, J.C., Jansen, E., Labeyrie, L., Landais, A., Marti, O., Michel, E., Mosquet, E., Risebrobakken, B., Swingedouw, D., Waelbroeck, C. Northern ice sheet melting regulated Northern Hemisphere climate during the Last Interglacial, Earth and Planetary Science Letters, submitted for publication.

Hachikubo, A., Kosaka, T., Kida, M., Krylov, A., Sakagami, H., Minami, H., Takahashi, N., Shoji, H., 2007. Isotopic fractionation of methane and ethane hydrates between gas and hydrate phases. Geophysical Research Letters 34, L21502. doi:10.1029/2007GL030557.

Heinze, C., Maier-Reimer, E., Winn, K., 1991. Glacial pCO_2 reduction by the world ocean: experiments with the Hamburg carbon cycle model. Paleoceanography 6 (4), 395–430.

Hendy, I.L., Kennett, J.P., 2000. Stable isotope stratigraphy and paleoceanography of the last 170 K.Y.: site 1014, Tanner Basin, California. Proceedings of the Ocean Drilling Program. Scientific Results 167, 129–140.

Huybers, P., Wunsch, C., 2003. Rectification and precession signals in the climate system. Geophysical Research Letters 30 (19), 2011. doi:10.1029/2003GL017875.

Huybers, P., Wunsch, C., 2005. Obliquity pacing of the late Pleistocene glacial terminations. Nature 434, 491–494.

Imbrie, J., Hays, J.D., Martinson, D.G., McIntyre, A., Mix, A.C., Morley, J.J., Pisias, N.G., Prell, W.L., Shackleton, N.J., 1984. The orbital theory of Pleistocene climate: support from a revised chronology of the marine $\delta^{18}O$ record. In: Berger, A., Imbrie, J., Hays, H., Kukla, G., Saltzman, B. (Eds.), Milankovitch and Climate: Understanding the Response to Astronomical Forcing, Proceedings of the NATO Advanced Research Workshop held 30 November–4 December, 1982 in Palisades, NY. D. Reidel Publishing, Dordrecht, pp. 269–305.

Joos, F., Gerber, S., Prentice, I.C., Otto-Bliesner, B.L., Valdes, P.J., 2004. Transient simulations of Holocene atmospheric carbon dioxide and terrestrial carbon since the Last Glacial Maximum. Global Biogeochemical Cycles 18, GB2002. doi:10.1029/2003GB002156.

Joos, F., Spahni, R., 2008. Rates of change in natural and anthropogenic radiative forcing over the past 20,000 years. Proceedings of National Academy of Sciences 105, 1425–1430.

Jouzel, J., Masson-Delmotte, V., Cattani, O., Dreyfus, G., Falourd, S., Hoffmann, G., Minster, B., Nouet, J., Barnola, J.M., Chappellaz, J., Fischer, H., Gallet, J.C., Johnsen, S., Leuenberger, M., Loulergue, L., Luethi, D., Oerter, H., Parrenin, F., Raisbeck, G., Raynaud, D., Schilt, A., Schwander, J., Selmo, E., Souchez, R., Spahni, R., Stauffer, B., Steffensen, J.P., Stenni, B., Stocker, T.F., Tison, J.L., Werner, M., Wolff, E.W., 2007. Orbital and millennial Antarctic climate variability over the past 800,000 years. Science 317, 793–796.

Köhler, P., Fischer, H., Munhoven, G., Zeebe, R.E., 2005. Quantitative interpretation of atmospheric carbon records over the last glacial termination. Global Biogeochemical Cycles 19, GB4020. doi:10.1029/2004GB002345.

Köhler, P., Fischer, H., Schmitt, J., Munhoven, G., 2006. On the application and interpretation of Keeling plots in paleo climate research – deciphering $\delta^{13}C$ of atmospheric CO_2 measured in ice cores. Biogeosciences 3 (4), 539–556.

Köhler, P., Fischer, H., Schmitt, J., 2010. Atmospheric $\delta^{13}CO_2$ and its relation to pCO_2 and deep ocean δ13C during the late Pleistocene. Paleoceanography 25, PA1213. doi:10.1029/2008PA001703.

Lambert, F., Delmonte, B., Petit, J.R., Bigler, M., Kaufmann, P.R., Hutterli, M.A., Stocker, T.F., Ruth, U., Steffensen, J.P., Maggi, V., 2008. Dust-climate couplings over the past 800,000 years from the EPICA Dome C ice core. Nature 452, 616–619.

Lipenkov, V., Candaudap, F., Ravoire, J., Dulac, E., Raynaud, D., 1995. A new device for air content measurements in polar ice. Journal of Glaciology 41, 423–429.

Lototskaya, A., Ganssen, G.M., 1999. The structure of termination II (penultimate deglaciation and Eemian) in the North Atlantic. Quaternary Science Reviews 18, 1641–1654.

Loulergue, L., Parrenin, F., Blunier, T., Barnola, J.-M., Spahni, R., Schilt, A., Raisbeck, G., Chappellaz, J., 2007. New constraints on the gas age-ice age difference along the EPICA ice cores, 0–50 kyr. Climate of the Past 3, 527–540.

Loulergue, L., Schilt, A., Spahni, R., Masson-Delmotte, V., Blunier, T., Lemieux, B., Barnola, J.-M., Raynaud, D., Stocker, T.F., Chappellaz, J., 2008. Orbital and millennial-scale features of atmospheric CH_4 over the past 800,000 years. Nature 453, 383–386.

Lourantou, A., 2009. Constraints on the carbon dioxide deglacial rise based on its stable carbon isotopic ratio. PhD thesis, Université Joseph Fourier, pp. 194.

Lourantou, A., Lavrič, J.V., Köhler, P., Barnola, J.-M., Michel, E., Paillard, D., Raynaud, D., Chappellaz, D., 2010. A detailed carbon isotopic constraint on the causes of the deglacial CO2 increase. Global Biogeochemical Cycles 24 GB2015, doi:10.1029/2009GB003545.

Lüthi, D., Floch, M.L., Bereiter, B., Blunier, T., Barnola, J.-M., Siegenthaler, U., Raynaud, D., Jouzel, J., Fischer, H., Kawamura, K., Stocker, T.F., 2008. High-resolution carbon dioxide concentration record 650,000–800,000 years before present. Nature 453, 379–382.

Martin, J.H., 1990. Glacial–interglacial CO_2 change: the iron hypothesis. Paleoceanography 5 (1), 1–13.

Masson-Delmotte, V., Stenni, B., Pol, K., Braconnot, P., Cattani, O., Falourd, S., Kageyama, M., Jouzel, J., Landais, A., Minster, B., Barnola, J.M., Chappellaz, J., Krinner, G., Johnsen, S., Röthlisberger, R., Hansen, J., Mikolajewicz, U., Otto-Bliesner, B., 2010. EPICA Dome C record of glacial and interglacial intensities. Quaternary Science Reviews 29, 113–128.

Masson-Delmotte, V., Stenni, B., Blunier, T., Cattani, O., Chappellaz, J., Cheng, H., Dreyfus, G., Edwards, R.L., Falourd, S., Govin, A., Kawamura, K., Johnsen, S.J., Jouzel, J., Landais, A., Lemieux-Dudon, B., Lourantou, A., Marshall, G., Minster, B., Mudelsee, M., Pol, K., Röthlisberger, R., Selmo, E., Waelbroeck, C. An abrupt change of Antarctic moisture origin at the end of termination II. Proceedings of the National Academy of Sciences, in press, doi:10.1073/pnas.0914536107.

McManus, J.F., Bond, G.C., Broecker, W.S., Johnsen, S., Labeyrie, L., Higgins, S., 1994. High-resolution climate records from the North Atlantic during the last interglacial. Nature 371. doi:10.1038/371326a0.

Menviel, L., Timmermann, A., Mouchet, A., Timm, O., 2008. Meridional reorganizations of marine and terrestrial productivity during Heinrich events. Paleoceanography 23, PA1203. doi:10.1029/2007PA001445.

Molyneux, E.G., Hall, I.R., Zahn, R., Diz, P., 2007. Deep water variability on the southern Agulhas Plateau: interhemispheric links over the past 170 ka. Paleoceanography 22, PA4209. doi:10.1029/2006PA001407.

Monnin, E., Indermühle, A., Dällenbach, A., Flückiger, J., Stauffer, B., Stocker, T.F., Raynaud, D., Barnola, J.-M., 2001. Atmospheric CO_2 concentrations over the Last Glacial Termination. Science 291, 112–114.

Müller, U.C., Kukla, G.J., 2004. North Atlantic Current and European environments during the declining stage of the last interglacial. Geology 32, 1009–1012.

North Greenland Ice Core Project Members, 2004. High-resolution record of Northern Hemisphere climate extending into the last interglacial period. Nature 431, 147–151.

Ninnemann, U.S., Charles, C.D., 1997. Regional differences in Quaternary Subantarctic nutrient cycling: link to intermediate and deep water ventilation. Paleoceanography 12, 560–567.

Oppo, D.W., McManus, J.F., Cullen, J.L., 2006. Evolution and demise of the Last Interglacial warmth in the subpolar North Atlantic. Quaternary Science Reviews 25, 3268–3277.

Otto-Bliesner, B.L., Brandy, E.C., 2010. The sensitivity of the climate response to the magnitude and location of freshwater forcing: last glacial maximum experiments. Quaternary Science Reviews 29, 56–73.

Pahnke, K., Zahn, R., 2005. Southern hemisphere water mass conversion linked with North Atlantic climate variability. Science 307, 1741–1746.

Parrenin, F., Barnola, J.-M., Beer, J., Blunier, T., Castellano, E., Chappellaz, J., Dreyfus, G., Fischer, H., Fujita, S., Jouzel, J., Kawamura, K., Lemieux-Dudon, B., Loulergue, L., Masson-Delmotte, V., Narcisi, B., Petit, J.-R., Raisbeck, G., Raynaud, D., Ruth, U., Schwander, J., Severi, M., Spahni, R., Steffensen, J.P., Svensson, A., Udisti, R., Waelbroeck, C., Wolff, E., 2007. The EDC3 chronology for the EPICA Dome C ice core. Climate of the Past 3, 485–497.

Pena, L.D., Cacho, I., Ferretti, P., Hall, M.A., 2008. El Niño–Southern Oscillation-like variability during glacial terminations and interlatitudinal teleconnections. Paleoceanography 23, PA3101. doi:10.1029/2008PA001620.

Petit, J.R., Jouzel, J., Raynaud, D., Barkov, N.I., Barnola, J.-M., Basile, I., Bender, M., Chappellaz, J., Davis, M., Delaygue, G., Delmotte, M., Kotlyakov, V.M., Legrand, M., Lipenkov, V.Y., Lorius, C., Pépin, L., Ritz, C., Saltzman, E., Stievenard, M., 1999. Climate and atmospheric history of the past 420,000 years from the Vostok ice core, Antarctica. Nature 399, 429–436.

Raynaud, D., Lipenkov, V., Lemieux-Dudon, B., Duval, P., Loutre, M.-F., Lhomme, N., 2007. The local insolation signature of air content in Antarctic ice. A new step toward an absolute dating of ice records. Earth and Planetary Science Letters 261, 337–349.

Ridgwell, A.J., 2003. An end to the "rain ratio" reign? Geochemistry Geophysics Geosystems 4, 1051. doi:10.1029/2003GC000512.

Ridgwell, A.J., Watson, A.J., Archer, D.A., 2002. Modelling the response of the oceanic Si inventory to perturbation, and consequences for atmospheric CO_2. Global Biogeochemical Cycles 16 (4), 1071. doi:10.1029/2002GB001877.

Robinson, S.G., Maslin, M.A., McCave, I.N., 1995. Magnetic susceptibility variations in Upper Pleistocene deep-sea sediments of the NE Atlantic: implications for ice rafting and paleocirculation at the Last Glacial Maximum. Paleoceanography 10, 221–250.

Röthlisberger, R., Bigler, M., Wolff, E.W., Joos, F., Monnin, E., Hutterli, M.A., 2004. Ice core evidence for the extent of past atmospheric CO_2 change due to iron fertilisation. Geophysical Research Letters 31, L16207. doi:10.1029/2004GL020338.

Röthlisberger, R., Mudelsee, M., Bigler, M., de Angelis, M., Fischer, H., Hansson, M., Lambert, F., Masson-Delmotte, V., Sime, L., Udisti, R., Wolff, E.W., 2008. The southern hemisphere at glacial terminations: insights from the Dome C ice core. Climate of the Past 4, 345–356.

Sánchez-Goñi, M.F., Eynaud, F., Turon, J.L., Shackleton, N.J., 1999. High resolution palynological record off the Iberian margin: direct land–sea correlation for the Last Interglacial complex. Earth and Planetary Science Letters 171, 123–137.

Sarnthein, M., Tiedemann, R., 1990. Younger Dryas-style cooling events at glacial terminations I–VI at ODP Site 658: associated benthic $\delta^{13}C$ anomalies constrain meltwater hypothesis. Paleoceanography 5 (6), 1041–1055.

Schaefer, H., Lourantou, A., Barnola, J.-M., Raynaud, D., Chappellaz, J. On the suitability of partially clathrated ice for palaeoatmospheric $\delta^{13}C$ of CO_2 measurements, in preparation.

Schmittner, A., Brook, E., Ahn, J., 2007. Impact of the Ocean's overturning circulation on atmospheric CO_2. AGU Geophysical Monograph Series 173, 209–246.

Schulz, K.G., Zeebe, R.E., 2006. Pleistocene glacial terminations triggered by synchronous changes in Southern and Northern Hemisphere insolation: the insolation canon hypothesis. Earth and Planetary Science Letters 249, 326–336.

Seidenkrantz, M.-S., Bornmalm, L., Johnsen, S.J., Knudsen, K.L., Kuijpers, A., Lauritzen, S.-E., Leroy, S.A.G., Mergeal, I., Schweger, C., Vliet-Lanoë, B.V., 1996. Two-step deglaciation at the Oxygen Isotope Stage 6/5E transition: the Zeifen-Kattegat climate oscillation. Quaternary Science Reviews 15, 63–75.

Skinner, L.C., Shackleton, N.J., 2006. Deconstructing terminations I and II: revisiting the glacioeustatic paradigm based on deep-water temperature estimates. Quaternary Science Reviews 25, 3312–3321.

Spero, H.J., Lea, D.W., 2002. The cause of carbon isotope minimum events on glacial terminations. Science 296, 522–525.

Stauffer, B., Tschumi, J., 2000. Reconstruction of past CO_2 concentrations by ice core analyses. In: Hondoh, T. (Ed.), Physics of Ice Core Records. Hokkaido University Press, Sapporo, Japan, pp. 217–241.

Stephens, B.B., Keeling, R.F., 2000. The influence of Antarctic sea ice on glacial–interglacial CO_2 variations. Nature 404, 171–174.

Toggweiler, J.R., Russell, J.L., Carson, S.R., 2006. Midlatitude westerlies, atmospheric CO_2, and climate change during the ice ages. Paleoceanography 21, PA2005. doi:10.1029/2005PA001154.

Waelbroeck, C., Frank, N., Jouzel, J., Parrenin, F., Masson-Delmotte, V., Genty, D., 2008. Transferring radiometric dating of the last interglacial sea level high stand to marine and ice core records. Earth and Planetary Science Letters 265 (1–2), 183–194.

Wilson, A.T., Long, A., 1997. New approaches to CO_2 analysis in polar ice cores. Journal of Geophysical Research 102, 26601–26606.

Wolff, E.W., Fischer, H., Fundel, F., Ruth, U., Twarloh, B., Littot, G.C., Mulvaney, R., Rothlisberger, R., Angelis, M.D., Boutron, C.F., Hansson, M., Jonsell, U., Hutterli, M.A., Lambert, F., Kaufmann, P., Stauffer, B., Stocker, T.F., Steffensen, J.P., Bigler, M., Siggaard-Andersen, M.L., Udisti, R., Becagli, S., Castellano, E., Severi, M., Wagenbach, D., Barbante, C., Gabrielli, P., Gaspari, V., 2006. Southern Ocean sea-ice extent, productivity and iron flux over the past eight glacial cycles. Nature 440, 491–496.

Wolff, E.W., Fischer, H., Röthlisberger, R., 2009. Glacial terminations as southern warmings without northern control. Nature Geosciences 2, 206–209.

Zharkov, V., Nof, D., 2008. Agulhas ring injection into the South Atlantic during glacials and interglacials. Ocean Science 4, 223–237.